

Smart Patches : Self-monitoring composite patches for the repair of aircraft

Sam Crossley^{*a}, Zaira Marioli-Riga^b, George Tsamasphyros^c, George Kanderakis^c, Nikos Furnarakis^c, Aris Ikiades^d, Mary Konstantaki^d

^a AOS Technology Ltd, 46 Pate Rd, Melton Mowbray, Leics, LE13 0RG, United Kingdom

^b Hellenic Aerospace Industries SA, PO Box 23 320 09 Schimatari, Greece

^c National Technical University of Athens, 5 Iroon Polytechniomy Ave, Zografu, Athens, Greece

^d FORTH IESL PO Box 1527, Heraklion 711 10, Crete, Greece

ABSTRACT

Conventional aircraft repair techniques employ bolted or riveted metallic reinforcements, which frequently introduce additional stress concentrations leading to further cracking and creating areas difficult or impossible to inspect. Bonded composite repairs (“patches”) result in the elimination of stress concentrations caused by additional fastener holes, improved strength to weight ratio and present a sealed interface. This reduces even further the danger of corrosion and fretting under the repair, gives greater flexibility in design and lessens application time while lengthening fatigue life. Embedding optical fibres and sensors into the patch, and combining this with advanced data collection and processing systems, creating a so-called “smart patch”, will enable the real-time assessment of aircraft structural integrity resulting in reliable prediction of maintenance requirements for repaired structures. This paper describes the current state of the art in smart patch technology, and includes a detailed description of the measurement problem and of the work being undertaken to solve it, at both the component and system level. An analysis of typical crack behaviour, based on FE modelling is presented and this demonstrates the need for optical strain sensors having a very short gauge length. The paper discusses the advantages and limitations of very short Fibre Bragg Gratings (FBGs) in this context and also provides early experimental data from 1mm and 2mm gratings which have been fabricated for this purpose. The paper also describes the impact of the measurement and environmental constraints on the design of the FBG interrogation system and presents the results of initial trials. The work is being undertaken in the framework of a collaborative project (ACIDS) which is co-funded by the European Commission

Keywords: Smart structures, aircraft repair, self-sensing, Bragg gratings, FBG interrogation

1. INTRODUCTION

Current economic world conditions are forcing to the operation of both military and civilian aircraft well beyond their original design life, resulting in innovative repair techniques. The recent development of high strength fibres and adhesives has led to the invention of a new methodology for the repair of metallic structures by the adhesive bonding of patches manufactured by composite materials. Bonded repairs are mechanically efficient, cost effective and can be applied rapidly to produce an inspectable damage tolerant repair [1-4]. The actual objective of the repair of a cracked or corroded metallic structure by an adhesively bonded composite patch is, practically, the transfer of loads from the one side of the sound material to the other via the patch, deviating the damaged area. Traditionally, structural problems due to fatigue or corrosion have been repaired by the addition of a metallic patch manufactured from aluminium or steel, which was mechanically joined to the cracked structure using fasteners or bolts. This kind of repair creates stress concentration areas at the vicinity of the fasteners, which may lead to further structural problems, like reduction of the fatigue life of the structure, etc. With the new technique the patch is manufactured using carbon / epoxy or boron / epoxy composite materials, while its bonding on the structure is performed by high strength adhesives. The load transfer from the

* sdc@aost.co.uk tel +44 1664 567711 fax +44 1664 56712

component to the patch and vice versa is achieved by the shear stresses applied on the adhesive layer. Subsequently, no extra holes are required in the vicinity of the crack and no stress concentration points are created. Moreover, the application of such a repair is faster than a traditional one, while the performance of non-destructive inspections of the main structure is possible without removing the patch [5].

In order to enable on line monitoring of the local stress field into a composite patch during the expected cracked propagation, optical fiber sensors can be structurally integrated into it. Fiber optic sensors present significant advantages, compared to other techniques in the area of stress-strain monitoring (e.g. strain gages, etc.), mainly concerning their extremely small size, the resistance to corrosion and fatigue, their immunity to electrical interference, as well as their chemical and mechanical compatibility with composite materials. Optical fibers may serve both as sensors, by means of Bragg Gratings, and as conduits for the sensor signals and can be integrated in fiber sensor networks, for extended area monitoring. [6-7]. In [8] the efficiency and the effects of embedding optical fibers in different layers were studied. It has been concluded that the best position to embed optical fibers through-the-thickness of a laminated patch coincides to the neutral surface of the patch, according to the Rose's analytical equations [9].

2. SMART PATCH MODELLING AND TESTING

2.1 MODELLING WORK

The selection of the examined cases and the choice of the materials were driven by the actual repairs usually met in the field of aeronautics technology, where composite patch repairs are mainly applied. Therefore, a cracked thin aluminum alloy plate (Al 2024-T3, $t=6\text{mm}$, $E=72.0\text{GPa}$, $\nu=0,3$) representing an aircraft skin with a crack has been examined, over which a laminated patch, composed of eight lamina of boron-epoxy prepreg (Textron 5521, $t=0.125\text{mm}$ per ply, $E_1=207\text{GPa}$, $E_2=E_3=19\text{GPa}$), was bonded using some high-performance film adhesive ($t=0.1\text{mm}$, $E=4.0$, $\nu=0,35$). The repair was supposed to bear mainly tensile loads coming from the far end of the metallic sheet, in a direction transverse to the crack. The basic geometrical characteristics of the repair case are shown in Figure 1.

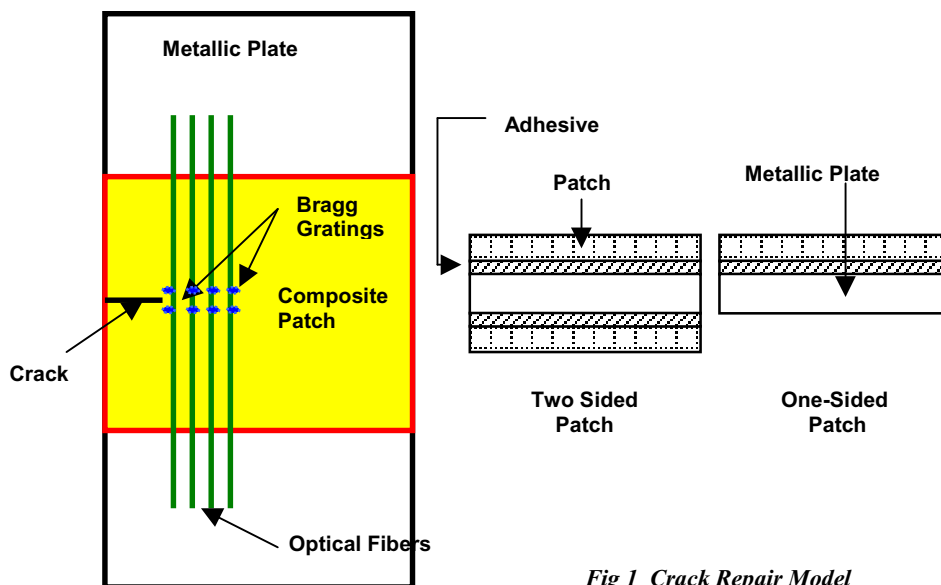


Fig 1 Crack Repair Model

The direction of the optical fibers was coincident to the direction of the loads and vertical to the crack. Optical fibers ($E=72.9, \nu=0,3$) were assumed to be bonded at the external surface of the composite patch, to avoid any interaction between them and the patch material (resin pocket forming around the fiber during manufacturing, stress concentrations etc.[10]). Their diameter ($100\mu\text{m}$) was approximately equal to the thickness of each lamina ($125\mu\text{m}$). Different optical

fiber paths and sensor positions were considered to study their ability to measure the developed strain field and to trace the position of the crack tip.

All the models were created using ANSYS finite element analysis software. Only 1/2 of the actual repair was modeled, because of symmetry, applying the required symmetry boundary conditions. The model was constructed from two main entities: the repaired structure (aluminum, patch and adhesive) and the optical fibers. The first entity was built using approximately 7000 3D SOLID 45 structural solid

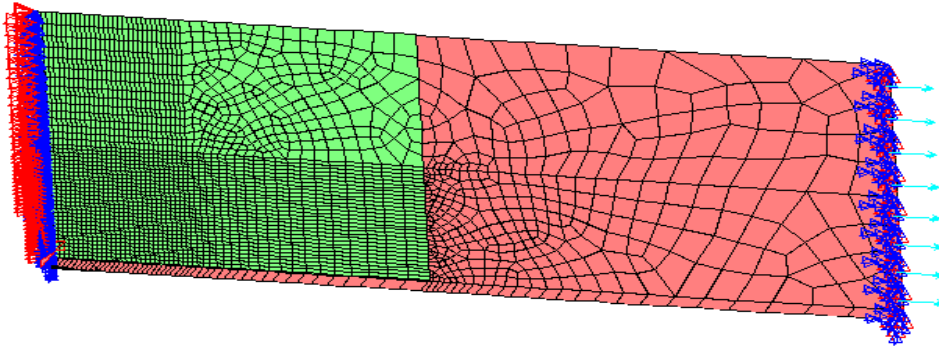


Figure 2: Overall view of the composite patch repair model with embedded optical fibers and applied boundary conditions. The straight horizontal lines define the optical fibers paths.

elements (common 8-node three-dimensional elements with three degrees of freedom at each node in translational directions – UX, UY, UZ [11]). One layer of these elements was defined to model each different material (metallic plate, adhesive layer and composite patch). Connectivity of the elements was established by using common nodes at the interfaces of the elements with different material properties. For the modeling of the optical fibers one-dimensional, LINK 8 elements defined by two nodes with three degrees of freedom (UX, UY, UZ) were used [11]. The spar elements were defined between existing nodes, at the external side of the composite patch.

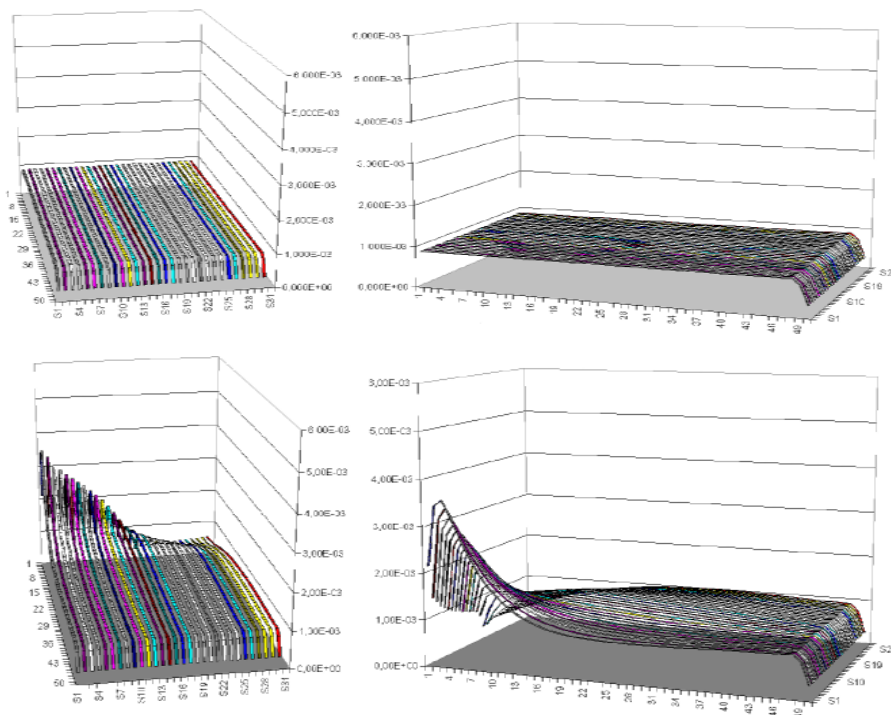


Figure 3: Graphical presentation of developed strains along the optical fibers for the case of an uncracked (upper) and a 15mm cracked (lower) single patched specimen

The modulus of elasticity and the area of the optical fiber were defined for each element as real constants, according to the corresponding values of the actual optical fibers. The optical fibers were defined on the straight lines formed by the nodes of the 3D elements, as shown in Figure 2. It should be noted that the arrangement of the solid elements was performed by dividing the concerned volume into parts which corresponded to the optical fiber paths. This way, the definition of a network of straight optical fibers was enabled and the simultaneous examination of 30 different paths could be performed. The crack was modeled by leaving the related edge nodes of the metallic substrate unconstrained, while the nodes of the composite patch were properly connected to the rest of the material. The force was applied as pressure far away from the repair to ensure that the area of interest is beyond any transition effects. An overall view of composite patch repair model with embedded optical fibers and applied boundary conditions is presented in Figure 2, while the results of computed strains of the uncracked and the cracked specimen are presented in Figure 3.

As far as the distribution of stresses through the thickness of the patch is concerned, and in order to avoid stress concentrations in the patch ends, due to shear lag phenomena, a stepped profile has been adopted with a 6.7% stepping ratio ($\text{length ply}_i / \text{length ply}_{i+1}$), as in the real repair procedure. The embedded optical fibers are supposed to be imported between the laminates of the prepreg that form the patch during the manufacturing process, and located at the vertical projection of the aluminum crack tip. Due to the unidirectional assumption of the patch stacking sequence a minimized resin pocket is formed around the fiber during manufacturing. The embedding direction is parallel to the loading axis, so as to trace the variations of the strain field in the direction of the applied loads. The lamina thickness was approximately equal to the optical fiber diameter ($100\mu\text{m}$), resulting to a plate-to-patch thickness ratio of 3.

Table 1: Examined Cases

Case No	1	2	3	4	5
Opt.Fiber Location	Between Laminas 1-2	Between Laminas 2-3	Between Laminas 3-4	Between Laminas 4-5	Between Laminas 5-6

Different locations of the optical fibers, presenting the possible embedding configurations, were assumed. Therefore, five different models were developed each one representing a different position of fiber embedding and different test case (table 1): between laminas 1-2, 2-3, 3-4, 4-5, 5-6 (Figure 4) and were compared to a similar model, without embedded optical fiber.

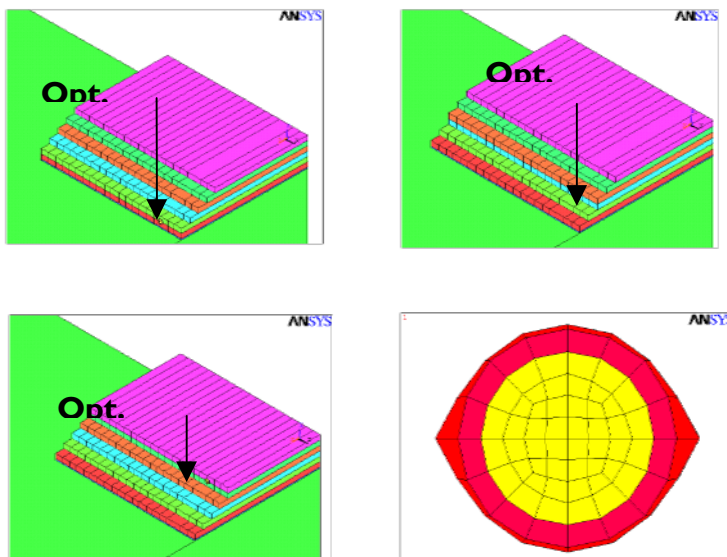


Figure 4: Optical fiber between laminas a) 1-2, b) 3-4, c) 5-6 and d) optical fiber/resin pocket modeling

The results obtained from the above-mentioned models led to several important issues, concerning the design technique of an embedded optical fiber system in a composite patch, in order to avoid strength weakening of the patch or, generally, any field-related phenomena that would lead to important structural degradation issues.

The maximum Von Mises stress field components due to the embedding of the optical fiber at various layers may be calculated and used to the non-dimensional change in maximum stress distribution as;

$$R_{vm} = \frac{S_{VonMises}^f - S_{VonMises}^0}{S_{VonMises}^0} \quad (1)$$

Is being defined, where $S_{VonMises}^f$ stands for the maximum Von Misses stress at the corresponding layer with an optical fiber embedded in the patch and $S_{VonMises}^0$ stands for the maximum Von Misses stress at the same layer for a patch with no optical fiber embedded. This ratio corresponds to the non-dimensional change in maximum stress distribution (according to the Von Misses Criterion) of the corresponding lamina as compared to the value of a similar patch without an embedded fiber. A graphical presentation of the through-the-thickness distribution of the ratio is shown in Figure 5

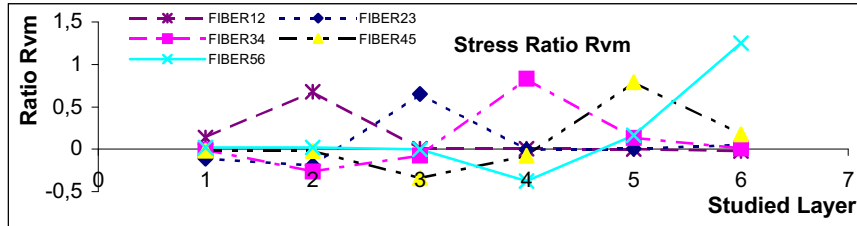


Figure 5: Through-the-thickness distribution of R_{vm} ratio (SUPC)

From these results it is obvious that as the fiber is being embedded to the outer layers the disturbance in stress field is higher than if the fiber is being embedded in the inner layers. On the other hand, the fiber has to be close to the high stress gradient area in order to measure efficiently the disturbed field. Also, even though the ratio shows that embedding to inner layers would be more secure (from a repair integrity point of view), the absolute values for stresses at the first layer shows that this is not the case, because there is a much greater gradient compared to the outer layers which multiplied with the above ratio present higher stress field values, as shown in Figure 6.

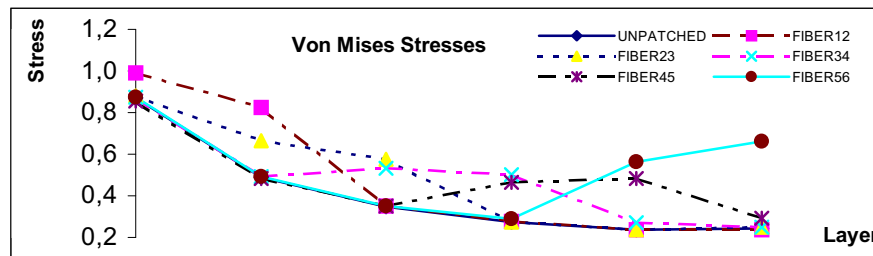


Figure 6: Maximum Stress distribution through patch layers (SUPC)

It is obvious from the above plot that wherever the fiber is being embedded to, the first layer will present high stress gradients, because of the stiffness mismatch of the repair and the load transfer area. Therefore, embedding an optical fiber in between first and second layer would cause an increase in maximum stress (in absolute values) as shown in the above graph that would exceed the non-fiber configuration stresses by 68%.

Calculating the neutral surface for the modeled configuration, according to equation (1), it reveals that its position would be in between the third and the fourth layer. A close study to the results of Table 2 would show that stress values in the layers below and above the optical fiber depend mainly on whether the fiber is above or below this neutral position. Clearly, if the fiber is below the neutral position then the stresses in the below layer are higher than the stresses in the layer above it and vice versa. Combining these results and studying closely the results of Figure 6 it is concluded that the best available position for embedding the optical fiber is between the layers 3-4 or the layers 4-5. The first position coincides to the neutral surface and the second is slightly above the neutral surface, as it is calculated by Rose's field equations. Both locations result in the minimum stress field perturbation, as compared to the non-fiber patch and the high stress gradient area of the first layer.

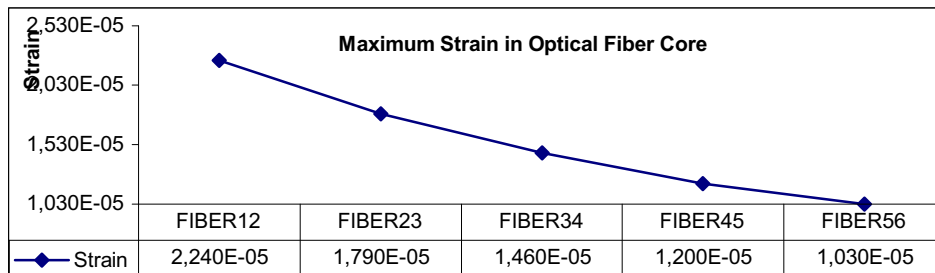


Figure 7: Maximum Strain in Optical Fiber Core (SUPC)

The corresponding maximum axial strains in the optical fiber core are presented in Figure 7. It is obvious that as the fiber moves to the outer layers the strain measured in the core and therefore its sensitivity becomes less as compared to the case of embedding in between the first and second layers. For the case of embedding the fiber in between the third-fourth or the fourth-fifth layer it would be preferable to choose the first one, as it would increase the sensitivity capability of the fiber as compared to the second choice by 20%.

Summarizing the above results from an engineering point of view and by close examination of a number of different factors that affect the life of the repair, as well as the sensing ability of the fiber, it is concluded that the best available embedding position of an optical fiber in a laminated patch, in the case of the single Unidirectional Patch Configuration, coincides to the location predicted as neutral surface position, according to the Rose's equation (1).

2.2 COUPON TESTS

In order to evaluate the numerical results and verify the structural integrity of the smart patch, a series of test coupons were designed and developed. The coupons, a schematic diagram of which is presented in Figure 8, were developed in order to study the structural integrity of the composite patch before and after the embedding of the optical fibers as well as the capability of the optical sensor to trace the alternations of the mechanical field at the strain gradient area.

The metallic - composite coupon was manufactured using aluminium 2024-T3 as the base structure under repair, having a crack of 10mm length. An adhesively bonded 7 layer patch was placed above the cracked area as a repair, developed using boron prepreg material with a O₇ lay-up. According to the previous numerical results, the fiber was embedded in parallel with the structural fibers of the laminas in order to minimize the resin

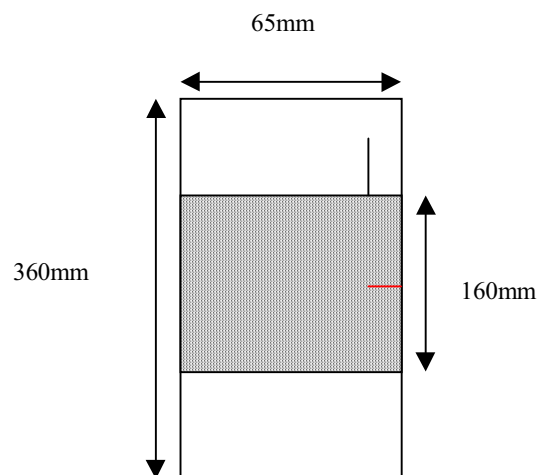


Fig 8 Test Coupon

pocket in the area of the fiber. Moreover, using the same results, the Bragg Grating optical sensor was placed in the area of the highest strain gradient which stands at the vertical axis of the crack tip of the aluminum. The coupons were loaded using an Instron tensile machine to various tensile loading levels up to 10KN's. The sensor was 2mm long having $\lambda_B=1539.117$, $\Delta\lambda=0.767$ and Reflectivity=94%. For these tests the sensor interrogation was performed using a Micron Optics FBG-IS interrogator, capable to trace the wavelength variations of the transmitted light in the fiber, due to the mechanical loading.

A main issue to be solved during the embedding process of the optical sensor as well as during the experimental testing, was the optical fiber-composite interface at the ingress/egress point. In order to prevent any fiber breakage, metallic protectors as the one presented in Figure 9 were used.

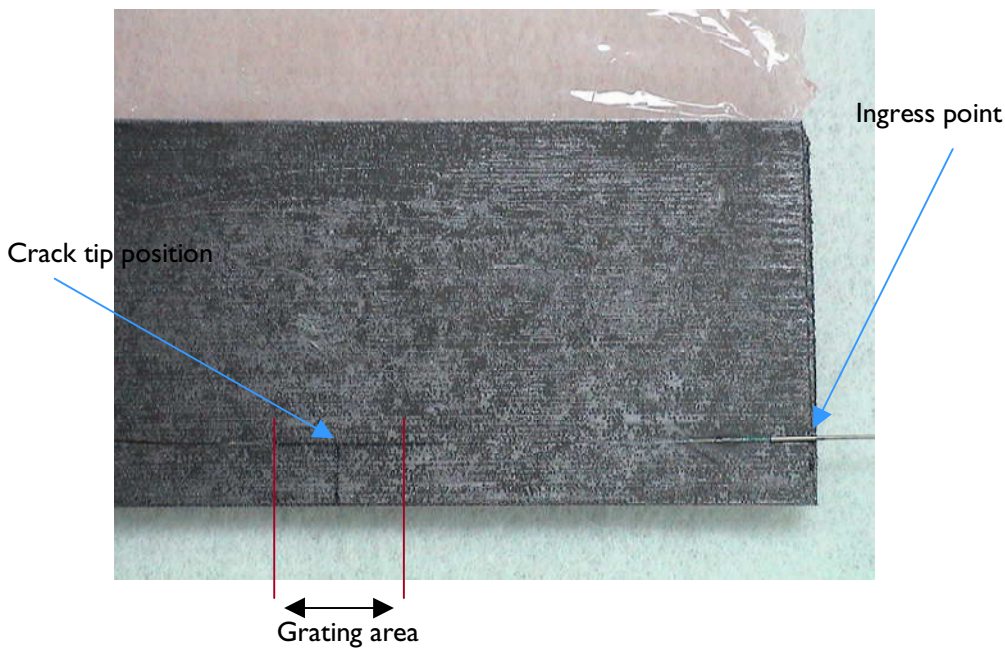


Figure 9: Optical sensor embedding in smart patch

The specimens were loaded up 10KN using tensile loading and various measurements were taken from the optical Bragg Grating sensor in order to study the traced mechanical field.

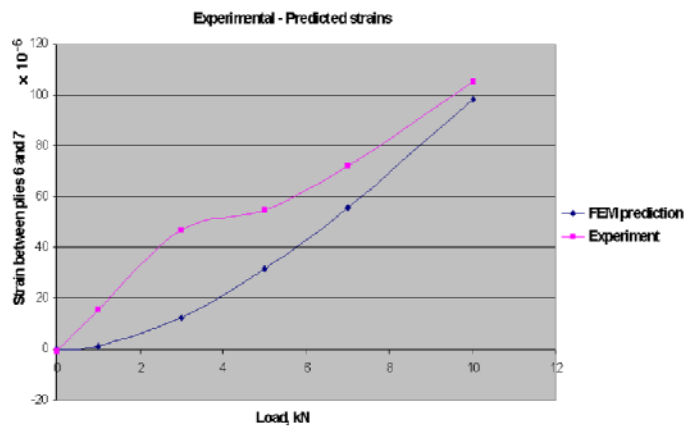
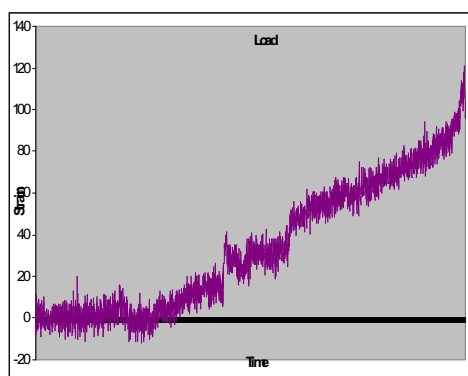


Figure 10: Strain measured by Micron Optics FBG-IS and comparison between numerical and experimental analysis

The results of the mechanical tests presented a good correlation between the numerical and experimental results, as may be seen from Figure 10 show that the predicted strain field was finally proved by the experimental tests with an error of less than 5%.

3. SHORT FIBRE BRAGG GRATINGS (SFBG)

Because the predicted range over which the strain field exists within the patch is very short, it is necessary to use a strain sensor with a very short gauge length. To this end, we proposed and demonstrated the fabrication and use of a very short (1-3mm) fibre Bragg grating, or SFBG

3.1 INSCRIPTION AND CHARACTERISTICS OF SFBGS

For the inscription of the FBGs a 25mm long phase mask with a pitch length of 1059,7 nm was used [12]. A KrF excimer laser was employed, emitting pulses with 20ns duration at 248 nm. The beam profile had a rectangular shape with dimensions of 31×14 mm² and was focused by a cylindrical lens with a focal length of 20 cm. A cylindrical lens was used focus the Excimer laser beam on the fibre and an optical aperture was also used to reduce the length of fibre illuminated by the beam. The fiber was placed almost in contact with the phase mask and along the line of maximum intensity of the beam. The UV laser energy fluence on the fiber was 92 mJ / cm² per pulse.

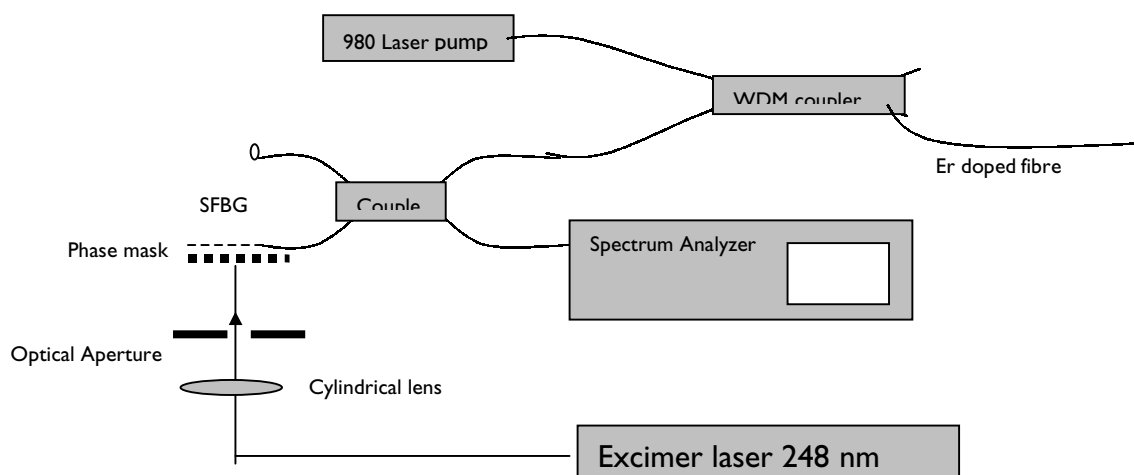


Fig 11 SFBG inscription

The backward fluorescence of an erbium-doped fiber was used as a broadband source in order to monitor the SFBG inscription process in real time(Figure 11). The photosensitive fibers were spliced on one of the output ports of a 3 dB coupler, enabling the simultaneous measurement of the reflected and transmitted spectra. The evolution of the grating was monitored using an optical spectral analyzer (OSA) to measure the increase of the reflected optical power at the Bragg wavelength. In addition the spectral broadening of the reflected signal was also measured at the Full Width Half Maximum (FWHM), during the inscription of the SFBG. Similarly the reflectivity of the SFBG was monitored by measuring the decrease in the transmission spectrum at the Bragg wavelength. All the SFBGs were written with the same energy fluence per pulses (92 mJ/cm²) and pulse repetition rates of 2 to 10 Hz.

The photosensitivity of a variety of fibers has been investigated including germanosilicate fibers with standard or increased germanium concentration and fibers with dopants such as boron or deuterium. Boron co-doped fiber has an excellent photosensitive response much greater than a fiber with an equivalent germanium concentration [13]. Hydrogen loading is often used to generate or significantly enhance the photosensitivity of various types of optical fibers and high reflectivities have been reported with hydrogenated boron co-doped fibers.

The experimental results showed that up to 140 J/cm^2 the fibers exhibit similar photosensitivity. For higher accumulated fluences the effect seems to be more pronounced in the case of the boron co doped fiber since after hydrogenation the photoinduced refractive index change continues to increase with the accumulate fluence even above 230 J/cm^2 and shows signs of saturation only above 400 J/cm^2 . Under this fluence the increase in the refractive index of the B/Ge fiber is around $2.7 \times 10^{-3} \text{ J/cm}^2$, which is an increase of almost an order of magnitude compared to the unloaded fiber. For the same level of accumulated fluence the hydrogenated high Ge fiber exhibits an index change of $1.9 \times 10^{-3} \text{ J/cm}^2$ [14].

Based on these results hydrogenated Boron co-doped germanosilicate fibre with 20mol% Germanium concentration was adopted. The fibre was placed in a hydrogen chamber at 160 Atm for 30 days in order to increase the their photosensitivity [14].

Several sets of 2 mm and 1 mm gratings were inscribed and a typical transmission and reflections spectrum for a 1mm SFBG is Fig 12 below using Hydrogenated Boron co-doped fibre. In the case of the 2 mm SFBG the reflectivity was about 87%, and is depended on the hydrogenation and laser exposure time. The central wavelength is 1556 nm with a FWHM of 0.66 nm and side band separation of 1.31 nm and about 10 % of the peak reflectance.

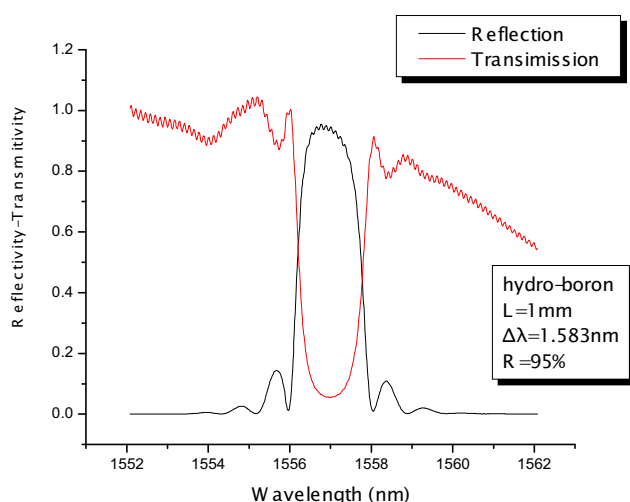


Fig 12 1mm SFBG

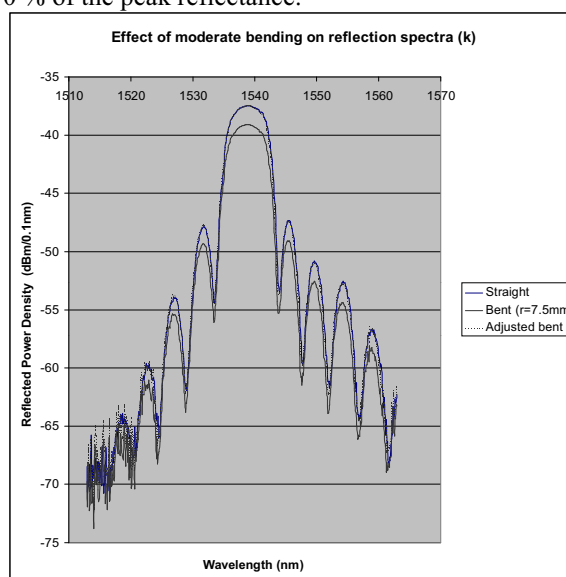


Fig 13 SFBG Deployment issues

Similarly for the 1 mm FBG the reflectivity is about 95% due to the longer exposure of the fibre to the UV laser light. The central wavelength is again 1556 nm with a FWHM of 1.58 nm and side band separation is 2.73 nm and about 15% of the peak reflectance.

As would be expected from a grating with a very small number of elements, the bandwidth is large; in this case, the 3dB bandwidth is approximately 2nm, a considerable, but inevitable drawback for an application where serial addressing is desirable. The sidelobe magnitude is approximately 10dB down on the central peak, but with a typical insertion loss of 0.6dB, this is not a significant factor in determining the maximum number of gratings that can be accommodated. The strain response of the SFBG is extremely close to linear

3.2 SFBG DEPLOYMENT ISSUES

One of the issues of concern in the use of SFBG is their increased sensitivity to deployment-induced changes in their spectral characteristics. To investigate this, the SFBG spectrum was recorded whilst the grating was lying undisturbed on the optical bench and in the second case, then the grating was “wrapped” around a mandrel of 15mm diameter. Figure 13 shows the two spectra superimposed, from which the bend-induced loss – of approximately 2.5dB - can clearly be identified. The figure also depicts a third curve, for which the bend-loss is mathematically-compensated. The difference

between this curve and the undisturbed fibre case, is practically indiscernible and indeed a difference analysis (note presented here) shows that bend-induced spectral modification is at a very minor level

4. SFBG INTERROGATION

The responsibility for the design and delivery of the SFBG interrogation system within the ACIDS project is principally that of AOS Technology Ltd, a UK SME company. AOS has been involved in the design and development of a number of conventional FBG interrogation systems. Most recently, AOS has launched the k-SCAN instrument, which can interrogate simultaneously up to 16 independent channels of up to 20 FBGs at more than 6kHz.



If more than one grating is located in a single channel, then these must either be physically separated, so that time-of-flight discrimination can be used to distinguish between them, or more commonly, they must each occupy a unique wavelength space, so that they can be accessed by wavelength tuning. In order to serially-access a number of FBGs, the k-SCAN instrument incorporates a tunable narrowband filter, which, in common with most of these components, is based on a Fabry-Perot designs. To achieve the fast update rate, k-SCAN uses a silicon MEM device, which is capable of scanning at many 10's of kHz.

Figure 14 AOS k-SCAN FBG interrogator

4.1 SYSTEM IMPLICATIONS FOR SMART PATCH APPLICATIONS

For the ACIDS application, the fast up-date rate of the k-SCAN instrument is not especially advantageous, but of critical importance is the long term stability and repeatability of the data, which is inherently difficult to achieve with this scanning methodology. The key to securing adequate stability and repeatability within the constraints of the original instrument design, was to radically improve the temperature control of several main system components, principally the optical source and most importantly, the tunable optical filter. The latter is a highly temperature-sensitive device, as may be seen from Fig 15, which shows how the centre wavelength of the filter passband varies as a function of package temperature, with a coefficient of approximately 1.6nm/°C. The MEM filter chip is mounted on a Peltier element which can be used to regulate its temperature. The original k-SCAN instrument incorporated this element within a closed loop controller based on the HYTEK HY5610 thick-film integrated controller. Whilst this is adequate for high update rate applications, such as vibration analysis, it does not provide a performance level commensurate with the needs of extended monitoring, such as required by the Smart Patch deployment. The first task was therefore to re-

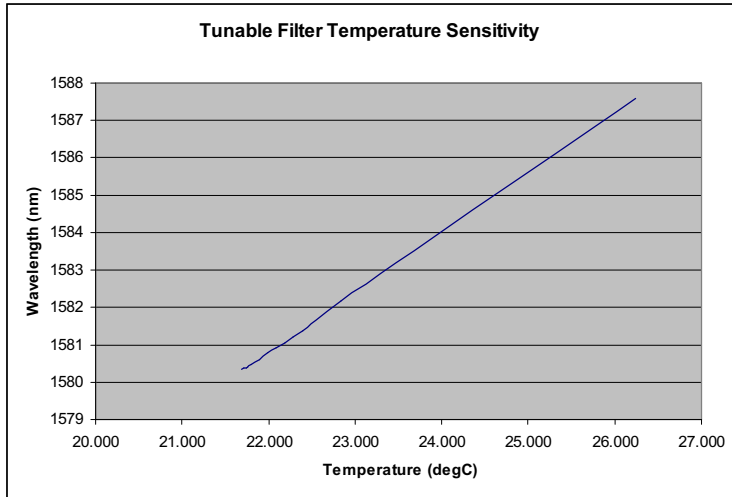


Figure 15 Filter Temperature Sensitivity

design the Peltier controller to provide significantly improved performance. A design based on the Maxim 1968 integrated controller was undertaken and the resulting performance gain – of the order of x10 - can be seen with reference to Fig 16, which shows the controller response to a step change in load.

With the re-designed controller, the temperature of the tunable filter chip can be maintained to better than 0.005°C (and probably to 0.001°C). Whilst the improved controller performance is significant in the overall system stability enhancement, several other steps were necessary to provide adequate overall thermal management, including a re-design

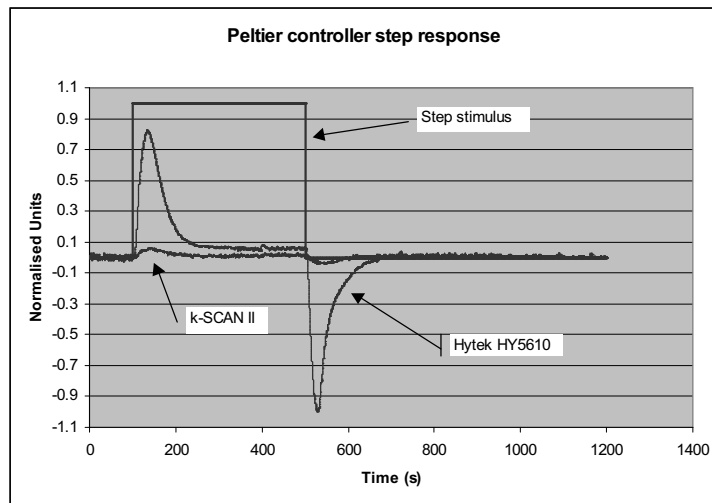


Figure 16 Improved controller response

of the mounting system for the tunable filter (to remove conducted thermal and mechanical loading effects) and the provision of a thermally controlled outer shielding for the filter, to maintain local temperature to a nominal level. The combined result of the various improvements discussed above, is that stability of the instrument is now sub-pm, which typically translates to a sub-microstrain level strain stability.

5. CONCLUSIONS

The technology of Smart Patch repair for aerostructures, as part of the EU co-funded project, “ACIDS” is described. This involves the use of very thin composite patches which are bonded onto the surface to be repaired. Fibre Bragg gratings embedded into the patch enable its performance over time to be monitored

From the results described it was concluded that a fiber optics network is capable of tracing the critical parameters required for the monitoring of the structural integrity of composite patch reinforced structures (i.e. strains developed at the patch and position of the crack tip). However, the optical sensors should be located according to certain rules, in order to acquire reliable results. Two Bragg Grating sensors should be used at each side of the crack per optical fiber, to enable adequate monitoring of the strain field and the crack tip location. For the case of one-sided patched structures, optical sensors should be located 2-3mm far from the crack axis and repeated at regular intervals of 2-5mm away from the crack tip, (depending on the required accuracy) until the predicted crack propagation limit. For the two-sided patched structures the optical sensors should be placed closer to the crack axis (i.e. only 1mm away) keeping the same periodicity. The second row of sensors should be located approximately 5-7mm far from the first. In case the maximum permissible strain of the optical fibers is locally exceeded due to the imposed loading or because of its proximity to the crack tip, a relocation of the optical sensor could be considered, since the interrupted strain field extends to a distance of almost 20mm away from the crack tip. Nevertheless, it should be noted that in such case the accuracy of the measurements might be slightly reduced, especially in case that the crack axis direction is changing.

Because of the very local strain effects within the patch, the gratings must have a very short gauge length. The fabrication, performance and deployment issues associated with these short gratings, SFBGs, are described. For the inscription of SFBG, the following parameters are important in obtaining high reflectivities and relatively low sidebands.

- The fibre photosensitivity has to be high and as the experimental work showed hydrogenated Boron codoped fibres with one of the highest photosensitivity are suitable for this application.

- The use of anodized beam profile has to be employed in order to reduce the spectral sidebands, which can be a problem in multiplexing more than one SFBG. However this is not easily achieved by phase mask-aperturing, in such short gratings, and the use of more sophisticated scanning methods should be used to center-weight the fibre grating structure.

The SFBSs can be serially addressed by a tunable FBG interrogator. Modifications to a commercially-available interrogation system manufactured by one of the project partners (AOS Technology Ltd) to achieve enhanced stability and long term drift performance are described.

The project, which is now at the mid-term stage, now moves to a more detailed characterisation of the SFBG patches, deployment trials and further improvements to the interrogation system, with a view to improving portability and cost.

6. ACKNOWLEDGEMENTS

The support of the European Commission (G4RD-CT-2001-00612 Project ACIDS Air Conformal Ice Detection System) and of the other consortium partners is gratefully acknowledged.

FORTH is a multi-disciplinary government sponsored research organization, with seven institutes, including the Institute of Electronic Structures and Lasers which incorporates the FO sensor group. FORTH's work on FBGs was partly sponsored by the Hellenic Telecommunications Company (OTE). We particularly wish to acknowledge the help of our students especially George Tamiolakis (SFBG).

7. REFERENCES

1. Baker, A.A. and Jones R. 1988. *Bonded Repair of Aircraft Structures*, Martinus Nijhoff Publishers.
2. Z.P. Marioli-Riga, G.J. Tsamasphyros, G.N. Kanderakis, Development of a Method for A/C Emergency Repairs by Composite Patches, S.A. Paipetis, E.E. Gdoutos, (Xanthi 1997), Vol II 143-156
3. Baker A.A., Bonded Composite Repair of Metallic Aircraft Components – Overview of Australian Activities, *Composite Repair of Military Aircraft Structures*, AGARD CP-550, pp. 1-1 to 1-14, Seville, Spain (1994).
4. G.J. Tsamasphyros, G.N. Kanderakis, Z.P. Marioli-Riga, “Three-dimensional Finite Elements Analysis of Debonding and Thermal Effects Near the Crack-Tip of a Metal Structure Repaired by a Composite Patch”, *3th Nat. Cong. on Comput. Mech.*, M. Aravas, J.T. Katsikadelis (editors) Univ. of Thessaly, Vol II, pp.429-436, Volos, Greece (1999).
5. Z.P. Marioli-Riga, G.J. Tsamasphyros, G.N. Kanderakis, “Non Destructive Evaluation of the Crack Propagation under a Composite Patch Repair Using the Eddy Current Method”, *SPIE's 5th International Symposium on Nondestructive Evaluation and Health Monitoring of Ageing Infrastructure*, Newport Beach, CA, USA (2000).
6. Raymond Measures, “Fiber Optic Sensing for Comp. Smart Structures”, AGARD, CP-531, 1992.
7. J. Sirkis et al. “What do embedded optical fibers really measure?”, SPIE, Vol.1777, 1992, N. Spon Ltd, 1981, London & NY.
8. G.J. Tsamasphyros, N. K. Furnarakis, G.N. Kanderakis, Z.P. Marioli-Riga, “Three-Dimensional Finite Element Analysis of Composite Patches with Embedded Optical Fibres – Through Thickness Optimization”, ICCES 01, Puerto Vallarta, Mexico, 19-24 August 2001.
9. L.R.F. Rose Theoretical Analysis of Crack Patching in Baker A.A., Jones R., *Bonded Repair of Aircraft Structures*, Martinus Nijhoff Publishers, Dordrecht, (1988).
10. A.Dasgupta et al. “Prediction of resin pocket geometry for stress analysis of optical fibers embedded in laminated composites”, *Smart Materials and Structures*, 1(1992),101-107.
11. ANSYS Finite Element Analysis Programme, Elements Manual, SAS IP Inc, (1998).
12. K. O. Hill, B. Malo, F. Bilodeau, D. C. Johnson, J. Albert, *Appl. Phys. Lett.* 62 (1993) 1035-1037.
13. D.L. Williams, B.J. Ainslie, J.R. Armitage, R. Kashyap, R. Campbell, *Electron. Lett.* 29 (1993) 45-47.
14. M. Konstantaki, G. Tamiolakis, A. Argyris, A. Othonos and A. Ikiades, Submitted to *Opt. Communication*.